Enrichment of Armchair Carbon Nanotubes *via* Density Gradient Ultracentrifugation: Raman Spectroscopy Evidence

Erik H. Hároz,[†] William D. Rice,[†] Benjamin Y. Lu,[†] Saunab Ghosh,[‡] Robert H. Hauge,[‡] R. Bruce Weisman,[‡] Stephen K. Doorn,[§,*] and Junichiro Kono[†,*]

[†]Department of Electrical and Computer Engineering, and [‡]Department of Chemistry, Rice University, Houston, Texas 77005, and [§]Center for Integrated Nanotechnologies, Los Alamos National Laboratory, Los Alamos, New Mexico 87545

ABSTRACT We have used resonant Raman scattering spectroscopy to fully analyze the relative abundances of different (*n*,*m*) species in single-walled carbon nanotube samples that are metallically enriched by density gradient ultracentrifugation. Strikingly, the data clearly show that our density gradient ultracentrifugation process enriches the metallic fractions in armchair and near-armchair species. We observe that armchair carbon nanotubes constitute more than 50% of each (2*n* + *m*) family.

KEYWORDS: carbon nanotubes · armchair · separation · enrichment · ultracentrifugation · optical absorption · photoluminescence · resonant Raman scattering

As exceptional one-dimensional conductors, metallic single-walled carbon nanotubes are ideal candidates for a variety of electronic applications[1,2] such as nanocircuit components and power transmission cables. In particular, (*n*,*n*) chirality, or "armchair", metallic nanotubes are predicted to be truly gapless and intrinsically insensitive to disorder,[3,4] consistent with experimentally observed ballistic conduction behavior.[5,6] Unfortunately, progress toward such applications has been slowed by the inherent problem of nanotube synthesis whereby both semiconducting and metallic nanotubes are produced. Here, we use a metallic nanotube enrichment process based on a modified approach to the density gradient ultracentrifugation (DGU) technique first introduced by Arnold and co-workers[7,8] to create metallic-enriched nanotube samples. Using resonant Raman scattering spectroscopy, we have fully analyzed the relative abundances of the metallic species present in the sample both before and after DGU. Strikingly, the data clearly show that our DGU process enriches the metallic fractions in armchair and near-armchair species. While a similar trend has been previously reported,[9] using transmission electron microscopy nanodiffraction measurements of small statistical sampling, the present work constitutes the first macroscopic optical measurements of an ensemble of nanotubes, convincingly determining the relative population of each (*n*,*m*) species before and after DGU.

The DGU technique can separate as-produced nanotubes, suspended in aqueous solution by multiple surfactants and/or salts, based on conduction type, producing samples composed almost entirely of metallic or semiconducting nanotubes.[7,8,10,11] Typically, type purity has been assessed by a combination of photoluminescence excitation (PLE) spectroscopy and optical absorption spectroscopy[7,8,10,12] or by electrical conductivity measurements.[8,10,13−15] While PLE is a powerful approach, it can only be used to investigate semiconducting nanotubes. Moreover, broad overlapping peaks in absorption spectra and a lack of structural sensitivity in conductivity measurements make these techniques unsuitable for resolving the precise (*n*,*m*) makeup of metallic fractions. As a result, both absorption and conductivity measurements provide little information on the physical mechanism responsible for type-dependent enrichments.

Currently, resonant Raman scattering (RRS) spectroscopy is the only optical route to unambiguous assignments of metallic features to specific (*n*,*m*) species due to its ability to identify and correlate diameter-dependent phonons with chirality-specific optical transitions for all SWNTs. We present

*Address correspondence to kono@rice.edu, skdoorn@lanl.gov.

Received for review December 26, 2009 and accepted March 15, 2010.

Published online March 19, 2010. 10.1021/nn901908n

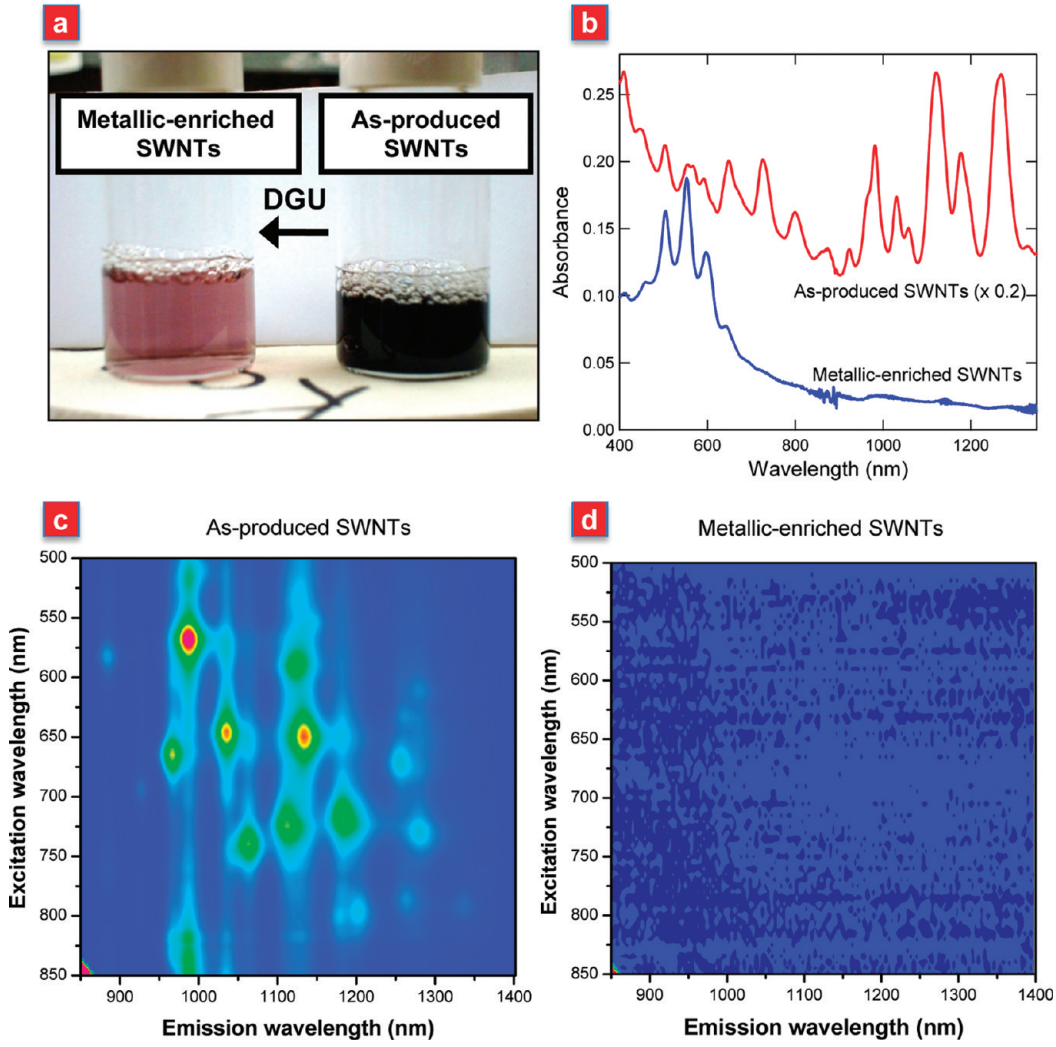

Figure 1. Comparison between as-produced and metallic-enriched single-walled carbon nanotube suspensions. (a) Typical metallic type enrichment (left) of HiPco SWNTs using density gradient ultracentrifugation compared to the as-produced HiPco material (right), both suspended in aqueous solution using surfactants. (b) Absorption spectra of metallic-enriched HiPco material and as-produced HiPco material. The as-produced material has been scaled by 0.2 for ease of comparison to the enriched material. A clear suppression of semiconducting absorption features (650−1300 nm) is evident as well as a sharpening of absorption features due to metallic nanotubes (450−650 nm) in the metallic-enriched SWNT sample as compared to as-produced SWNTs. (c,d) Photoluminescence excitation maps of as-produced HiPco (c) and metallic-enriched (d) HiPco materials. Signal in (d) has been scaled by 10 in photoluminescence intensity to show any possible weak features, and yet no signal could be observed from the metallic-enriched sample.

results of RRS measurements performed over a broad range of excitation wavelengths (440−850 nm) on the purest, topmost metallic-enriched fraction produced by DGU, such that all (*n*,*m*) species remaining in the enriched material were identified. When compared to as-produced single-walled carbon nanotubes (AP-SWNT) material, data from the metallic-enriched SWNT (ME-SWNT) sample indicate almost complete suppression of semiconducting SWNTs, confirming observations by PLE and absorption. Surprisingly, a comparison between the resonant Raman excitation profiles (REPs) of armchair SWNTs and the other metallic species indicates a *strong enrichment of species of large chiral angle (>19°) and, in particular, armchair SWNTs*. By combining results from such data, we have gained valuable insight into the phenomenological nature of DGU-based type separation.

RESULTS AND DISCUSSION

We followed the separation approach given by Yanagi *et al.*[10] with only small variations in sample dispersion conditions and fractionation (see Methods section). Figure 1a is a photograph of typical AP- and ME-SWNT materials, suspended in aqueous media using surfactant, whose absorption spectra are displayed in Figure 1b. The AP-SWNT spectrum shows well-defined peaks corresponding to the (*n*,*m*)-dependent, first, second, and third semiconducting [E_{11}^{S} (870−1600 nm), E_{22}^{S} (550−870 nm), and E_{33}^{S} (UV-490 nm)] and first metallic [E_{11}^{M} (440−670 nm)] optical transitions typical for

individualized HiPco SWNTs.[16] In contrast, the ME-SWNT spectrum shows no features in the E_{11}^S and E_{22}^S regions, indicative of the absence of semiconducting SWNTs. Also apparent is the increased peak-to-valley ratio in the E_{11}^M region of the ME-SWNTs, demonstrating a higher degree of individuality of the metallic chiralities and removal of the overlap between semiconducting and metallic peaks. An assessment of type purity can be determined by integrating the peak areas in the E_{11}^M and E_{22}^S regions.[8,10,12] This results in a metallic purity of ~98% for the ME-SWNT sample and 40% for the AP-SWNT sample. While such values are useful for determining the overall success of metallic enrichment, unknown baselines and overlapping absorption features make this technique unreliable. It can be immediately observed that the AP-SWNT and ME-SWNT samples are not of comparable nanotube concentrations with the ME-SWNT sample exhibiting lower absolute absorbance than the AP-SWNT sample. Despite this, the ME-SWNT sample exhibits strong and clear optical response toward excitations that probe metallic nanotubes and weak-to-no response toward excitations that probe semiconducting nanotubes. This is a consequence of metallic nanotube enrichment and not simply an overall low nanotube concentration effect, as is evidenced later.

The specific (*n*,*m*) semiconducting species remaining in the ME-SWNT sample can be determined *via* PLE.[16−18] Figure 1c,d shows PLE data for the AP-SWNT and ME-SWNT samples, respectively. While bright emission features emanate from the former (c), no emission above the detection threshold was detected from the latter (d), suggesting the absence of semiconducting SWNTs in ME-SWNT. One alternative explanation for the lack of emission is the extensive bundling of semiconducting nanotubes containing at least one metallic member, which would quench PL. However, the well-defined absorption features in the E_{11}^M region and the lack of any features in the E_{11}^S and E_{22}^S regions in Figure 1b (as well as the observation of very weak semiconducting Raman features under stronger excitation conditions; see Supporting Information)[19] exclude this possibility. Consequently, we can state that the ME-SWNT fraction consists almost entirely of metallic SWNT species (see Supporting Information for a complete discussion of semiconductors).[19]

RRS spectroscopy possesses the advantage of being able to detect all (*n*,*m*) species present, regardless of electronic type or aggregation state. By combining spectra obtained using a variety of excitation sources, all (*n*,*m*) species can be identified by correlating the resonance of the excitation wavelength to specific optical transitions with the diameter-dependent radial breathing mode (RBM) frequency.[20−22] Figure 2a,b plots RRS intensity for the AP-SWNT and ME-SWNT samples, respectively, as a function of excitation wavelength (562−670 nm) and Raman shift. For HiPco samples in this excitation range, RRS occurs for metallic and semiconducting SWNTs with diameters in the 0.95−1.36 and 0.68−0.90 nm ranges *via* E_{11}^M and E_{22}^S, respectively. In the ME-SWNT sample (Figure 2b), RBMs from small-diameter semiconductors [*e.g.*, (11,1), (7,5), (7,6), and (8,3)] are almost completely suppressed with the dominant contribution coming from metallic nanotubes of the $(2n + m) = 27$ and 30 families.

Further examination of the cluster of peaks of family 27 (insets in Figure 2a,b) reveals an unexpected change in the relative Raman intensities of the (*n*,*m*) members of family 27 between AP-SWNT and ME-SWNT. The strong peaks for the small-chiral-angle species [(11,5) and (12,3)] in AP-SWNT decrease in intensity through DGU, relative to the armchair (9,9) and near-armchair (10,7) species (see Figure 2b inset). At higher photon energies, this trend becomes even more selective. Figure 2c (AP-SWNT) and Figure 2d (ME-SWNT) show RRS from 445−500 nm, where resonances occur for small-diameter metallic nanotubes (0.72−0.95 nm) and larger-diameter semiconducting (0.97−1.36 nm) nanotubes *via* E_{11}^M and E_{33}^S, respectively. Again, strong suppression of semiconducting RBMs is clear, as well as suppression of some metallic RBMs. Closer examination of Figure 2c,d reveals that metallic enrichment of families 18 and 21 is mostly due to armchair nanotubes, with only the (7,7) and (6,6) species remaining in ME-SWNT. Suppression occurred for the (8,5) and (9,3) species of family 21 and the (7,4) and (8,2) species of family 18 [(9,3) was observed in AP-SWNTs *via* 514.5 nm discrete excitation].[19]

To quantify this chiral-angle-dependent metallic enrichment, we constructed REPs from the data contained in Figure 2. Figure 3a,b shows REPs for family 27 for AP-SWNT and ME-SWNT, respectively. The Raman intensity, I_{Raman}, for a particular RBM [*i.e.*, (*n*,*m*) species] can be written as a function of excitation energy E_{laser} such that

$$I_{Raman} = gN \times \left| \sum_{i,j} \frac{M_{e\text{-}o}^{g,i} M_{e\text{-}ph}^{g,i} M_{e\text{-}o}^{i,j}}{(E_{laser} - E_{ii} - i\gamma)(E_{laser} - E_{ii} - \hbar\omega_{ph} - i\gamma)} \right|^2 \quad (1)$$

where g is an experimental prefactor, N is the relative population of the (*n*,*m*) species probed, E_{ii} is the optical transition energy, γ is the electronic broadening factor, $\hbar\omega_{ph}$ is the phonon energy, $M_{e\text{-}ph}$ is the exciton−phonon coupling matrix element, $M_{e\text{-}o}$ is the exciton−photon coupling matrix element, and the summation is over electronic states.[23] We used eq 1 to analyze the REP data in Figure 3 to determine the relative (*n*,*m*) populations for families 27 and 30 for both AP-SWNT and ME-SWNT, and the results are summarized in Table 1. Briefly, relative (*n*,*m*) populations are determined by dividing experimental, at-resonance, (*n*,*m*)-specific Raman intensities by theo-

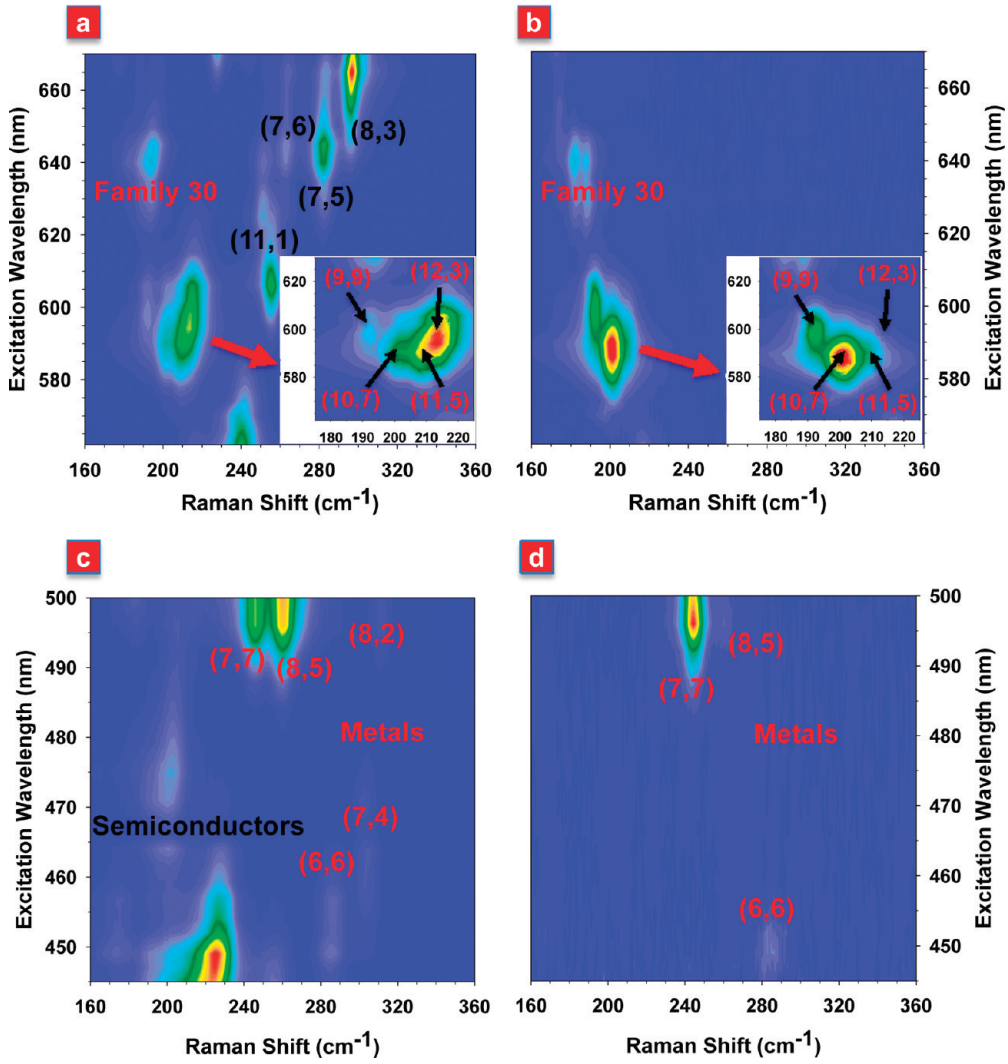

Figure 2. Resonant Raman scattering excitation maps demonstrating enrichment of armchair and near-armchair carbon nanotubes. (a,b) Resonant Raman scattering excitation maps of as-produced (a) and metallic-enriched (b) SWNT samples over an excitation range of 562−670 nm. The insets of (a) and (b) highlight family ($2n + m$) = 27. The scale of the inset of (a) has been magnified by 1.5 relative to the full excitation map to differentiate the (n,m) members of family 27 more clearly. (c,d) Resonant Raman scattering excitation maps of as-produced (c) and metallic-enriched (d) SWNT samples over an excitation range of 445−500 nm. Metallic (n,m) species are labeled in red, and semiconducting species are labeled in black. In both excitation ranges, a clear shift in relative Raman intensity occurs toward metallic (n,m) species of large chiral angle, namely, the armchair and near-armchair species.

retical, at-resonance, (n,m)-specific Raman intensities per unit length derived from exciton−photon and exciton−phonon coupling matrix elements calculated by Jiang *et al.*[23] Smaller-chiral-angle species show significant suppression, with the (12,3) registering no signal after DGU. In contrast, the armchair and near-armchair chiralities become the dominant elements, rising together from a relative population of 70 to 98% in family 27; analogous but less dramatic behavior is seen with family 30 (see Supporting Information for further details on population analysis).[19] The noticeably high relative armchair population, even in the AP-SWNT sample, is surprising but consistent with recent theoretical work suggesting that armchair nanotubes should be the most populous species in the distribution of nanotubes synthesized by several different methods.[24] Experimentally, this is difficult to verify because the armchair species have a weak Raman response due to their small exciton−phonon coupling and, as a result, are obscured by semiconducting tubes and other metallic tubes.[20,21,23,25−27]

A similar chiral trend in DGU-based, metallic enrichment has been previously reported by Sato *et al.*,[9] using transmission electron microscopy nanodiffraction measurements. However, the nature of this approach yields only a small statistical sampling of the entire sample. By employing RRS, we extracted information on nanotube ensembles with data that are an average over a macroscopic population of each (n,m) species. One important advantage of this is the ability to take an in-depth look at

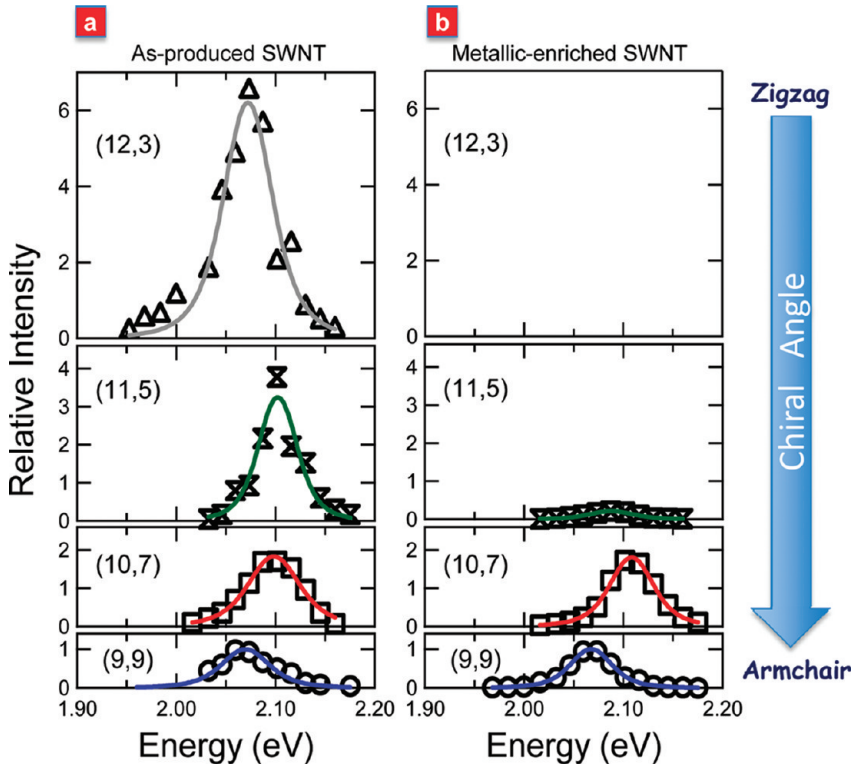

Figure 3. Resonant Raman excitation profiles for different (*n*,*m*) metallic nanotubes showing relative population change toward large chiral species *via* density gradient ultracentrifugation enrichment. (a) Raman excitation profiles (REPs) for the (*n*,*m*) members of family (2*n* + *m*) = 27 as observed in the as-produced SWNT sample. (b) Raman excitation profiles for the (*n*,*m*) members of family (2*n* + *m*) = 27 as observed in the metallic-enriched SWNT sample. The (12,3) is not displayed in (b) because an REP could not be constructed due to its extremely weak observation at only one excitation wavelength (586 nm). Near-zigzag species (12,3) and (11,5) see a marked decrease in intensity, while armchair (9,9) and near-armchair (10,7) species remain undisturbed by the DGU process.

armchair nanotubes as a macroscopic ensemble. Several previous studies[20,21,23,25,26] have noted the exceedingly small Raman signal for armchairs as compared to other metallic species, even of similar diameter, with some theoretical estimates showing that armchairs possess exciton−phonon couplings an order of magnitude smaller than zigzag and near-zigzag species of the same family.[23,26,27] Despite this, armchairs (6,6) through (11,11) are clearly displayed in ME-SWNT, as shown in Figure 4a,b. Of particular note is the clarity with which the armchairs may be observed in Figure 4b as compared to Figure 4a.

CONCLUSION

Taken together, we have clear evidence that in DGU armchair and large-chiral-angle (>19°) species

TABLE 1. Evidence for Enrichment of Armchair and Near-Armchair Carbon Nanotubes[a]

(*n*,*m*)	diameter (nm)	chiral angle (degree)	REP amplitude of family 2*n* + *m* (AP)	REP amplitude of family 2*n* + *m* (ME)	REP electronic broadening (AP) (meV)	REP electronic broadening (ME) (meV)	theoretical Raman intensity per unit length[b]	% population of family 2*n* + *m* (AP)	% population of family 2*n* + *m* (ME)
Family 27									
(9,9)	1.221	30	1.0	1.0	80	67	0.02	36%	52%
(10,7)	1.159	24.2	2.5	2.3	87	71	0.05	34%	46%
(11,5)	1.111	17.8	2.2	0.3	77	71	0.13	11%	2%
(12,3)	1.077	10.9	6.6	0[c]	81		0.24	18%	0%
Family 30									
(10,10)	1.357	30	1.0	1.0	90	83	0.01	40%	46%
(11,8)	1.294	24.8	1.2	1.8	72	76	0.03	16%	27%
(12,6)	1.244	19.1	5.2	5.5	95	109	0.09	22%	27%
(13,4)	1.206	13	8.0	0[c]	91		0.16	19%	0%
(14,2)	1.183	6.6	2.5	0[c]	66		0.24	4%	0%

[a]Tabulated data extracted from numerical fits to Raman excitation profiles of members of families (2*n* + *m*) = 27 and 30 for both the as-produced and metallic-enriched samples. [b]The (*n*,*m*)-dependent theoretical Raman intensities per unit length were extracted from data displayed in ref 23. [c]These species were only weakly observable at one or two excitation wavelengths near resonance, and as such, REPs could not be constructed for them.

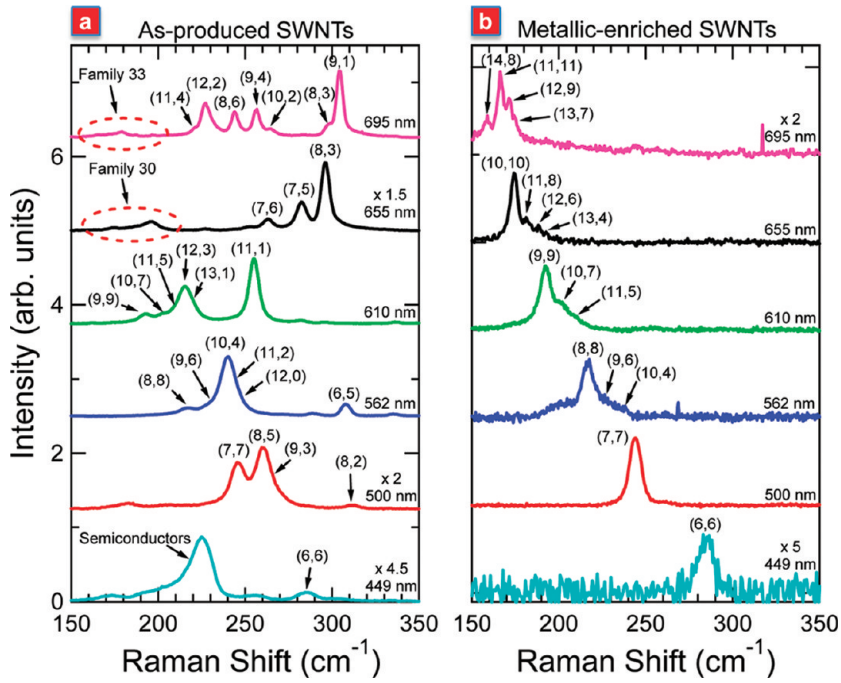

Figure 4. Suppression of semiconducting nanotubes and zigzag and near-zigzag metallic nanotubes. (a) Selected Raman spectra from data collected on the as-produced SWNT sample. (b) Selected Raman spectra from data collected on the metallic-enriched SWNT sample. These specific excitation wavelengths were chosen to highlight the armchair species. In (b), all semiconducting nanotubes are absent and small-chiral-angle metallic nanotubes are strongly suppressed, leaving only armchair and near-armchair nanotubes.

are enriched, while zigzag and near-zigzag metallic species and nearly all semiconductors are removed. One can hypothesize that such chiral angle selectivity might stem from a specificity in the nanotube interaction with one of the chiral surfactants, sodium cholate and/or sodium deoxycholate, which has been suggested by Green *et al.*[28] for enantiomer enrichment of left- and right-handed (6,5) nanotubes. While the achiral surfactant sodium dodecyl sulfate (SDS) has been shown to be necessary for metallic enrichment[8,10,11] [the DGU-based enrichments of Niyogi *et al.*,[11] which employ SDS and alkali salts (both achiral compounds), demonstrate enrichment of metallic species without any chiral angle bias], it may be the ease of stacking of the chiral surfactant onto the SWNT surface due to registry matching and sterics between the two that leads to the chiral angle selectivity.[29,30]

METHODS

Sample Preparation: Pristine, single-walled carbon nanotubes (SWNTs) were synthesized by the high-pressure carbon monoxide (HiPco) method at Rice University. The as-produced sample was produced by a variation of the standard ultracentrifugation technique.[16] HiPco SWNTs (batch HPR 188.1) were initially dispersed in 1% (wt/vol) sodium deoxycholate (DOC) (sodium deoxycholate monohydrate, Aldrich, 97% purity) in water by bath sonication (Cole-Parmer 60 W ultrasonic cleaner, model #08849-00) for 30 min, using a starting SWNT concentration of 200 mg/L. The suspension was then further sonicated by probe ultrasonicator (Cole-Parmer 500 W ultrasonic processor, model # CPX-600, 1/4 in. probe, 35% amplitude) for 30 min while being cooled in a water bath maintained at 10 °C. Finally, the suspension was centrifuged for 4 h at 109,500 g average (Sorvall Discovery 100SE Ultracentrifuge using a Sorvall AH-629 swing bucket rotor). After centrifugation, the upper 60% of the supernatant was removed (referred to in the main text as AP-SWNT) and used for optical measurements.

Samples enriched in metallic SWNTs were produced by the density gradient ultracentrifugation (DGU) technique employing a three-surfactant system.[10] HiPco SWNTs (batch HPR 188.1) were initially dispersed in 1% (wt/vol) DOC in water by bath sonication (Cole-Parmer 60W ultrasonic cleaner, model #08849-00) for 30 min. The starting concentration of SWNTs was 1 g/L. The suspension was then further sonicated by probe ultrasonicator (Cole-Parmer 500 W ultrasonic processor, model # CPX-600, 1/4 in. probe, 35% amplitude) for 17.5 h while being cooled in a water bath maintained at 10 °C. The suspension was then centrifuged for 1 h at 208 400*g* average (Sorvall Discovery 100SE Ultracentrifuge using a Beckman SW-41 Ti swing bucket rotor) to remove large bundles of SWNTs. After centrifugation, the upper 80% of the supernatant was removed for use in DGU. Unlike the procedure of Yanagi *et al.*,[10] the purification to remove amorphous carbon from the nanotube material through an 18 h ultracentrifugation after ultrasonication followed by resuspension into a 1% (wt/vol) DOC in water was not performed.

A mass density gradient was prepared composed of 1.5% (wt/vol) sodium dodecyl sulfate (SDS) (sodium dodecyl sulfate, molecular biology or electrophoresis grade, Sigma, 99% purity), 1.5% (wt/vol) sodium cholate (SC) (sodium cholate hydrate, Aldrich, 98% purity), and varying amounts of iodixanol (Opti-Prep density gradient medium, Sigma, 60% (wt/vol) solution in water). The gradient was layered inside a centrifuge tube in 2 mL volume steps starting from the bottom with 40, 30, 27.5, 25, 22.5, and 20% (wt/vol) iodixanol. All gradient steps except the 30% layer contained 1.5% (wt/vol) SDS and 1.5% (wt/vol) SC. The 30% layer, which contained SWNTs, was prepared by vortex mixing (Fisher Scientific Vortex Genie 2, model #12-812, mixed at maximum setting) for 2 min with 1 mL of the SWNT supernatant

prepared previously with 1 mL of 60% iodixanol, 2% SDS, and 2% SC to ultimately form 2 mL of 30% iodixanol, 1% SDS, 1% SC, and 0.5% DOC. The resulting suspension was immediately incorporated into the density gradient after the bottom 40% iodixanol layer was inserted into the centrifuge tube. The gradient was then centrifuged for 18 h at 208 400*g* average (Beckman SW-41 Ti swing bucket rotor). The resulting separated material was then removed by hand pipetting in 200 μL fractions with the most metallically enriched material appearing at the top of a resulting pink band. The topmost 200 μL fractions from the pink band of each centrifuge tube were combined together and then dialyzed into a 1% DOC (water) solution (Pierce, 3500D MW dialysis cassette). The resulting liquid (referred to in the main text as ME-SWNT) was used for all optical measurements. It should be pointed out, as is apparent after reading the above procedures, that the AP-SWNT sample is not the "parent" nanotube supernatant inserted into the density gradient to prepare the ME-SWNT sample, even though they are both derived from the same raw HiPco batch. Although the usage of the parent supernatant would be more ideal for studying the effect of DGU enrichment on the population distribution of (*n*,*m*) species, due to the high starting nanotube concentration of the parent supernatant, the suspension is unstable and exhibits bundling and precipitation of nanotubes after several days. As such, a more typical preparation of as-produced nanotubes in suspension was chosen so that the optical response of individualized nanotubes would be captured.

Optical Measurements: Optical absorption spectroscopy was performed in the 400−1350 nm range in 1 nm steps on an ultraviolet−visible−near-infrared, double beam spectrophotometer (Shimadzu UV-3101PC scanning spectrophotometer) through a 10 mm path length quartz cuvette using a 1% (wt/vol) DOC (water) reference.

Photoluminescence excitation spectroscopy was performed using excitation light with a 5 nm bandwidth in the wavelength range of 500−850 nm, obtained from a Xe lamp using a double monochromator (HORIBA Jobin-Yvon Fluorolog-3-211). Nanotube emission was measured from 850 to 1400 nm with a single-channel, cooled InGaAs detector *via* a monochromator with 6 nm band-pass filter. Spectra were acquired with 2.5 and 4.0 nm steps in excitation and emission wavelengths, respectively. Individual spectra were acquired with a 1 s per point integration time. Acquisitions were repeated, as required, to ensure reproducibility and to improve signal-to-noise ratio. Spectra were corrected for power and instrument response.

Resonant Raman spectroscopy was performed in a backscattering configuration with cw Ti:sapphire laser excitation, tunable dye laser excitation using Kiton Red and Rhodamine 6G dyes, Ar^+ ion laser discrete lines and frequency-doubled cw Ti:sapphire laser excitation scanned from 850−695, 680−610, 615−562, 514.5 and 501.7, and 500−440 nm, respectively. Excitation power was maintained at 25 mW. Individual Stokes shift spectra were obtained as 5 min integrations using a charge-coupled device camera mounted on a SPEX triple monochromator. The frequency of each carbon nanotube spectrum was calibrated at each excitation wavelength with the nonresonant Raman spectrum of 4-acetamidophenol. Intensities were corrected for instrument response using fits to the intensities of peaks of 4-acetamidophenol and scaling the nanotube radial breathing mode spectra by the average intensity value at each excitation wavelength. All Raman spectra were taken at room temperature and ambient pressure.

Acknowledgment. This work was supported by the DOE/BES through Grant No. DEFG02-06ER46308, the Robert A. Welch Foundation through Grant Nos. C-1509 and C-0807, the Air Force Research Laboratories under contract number FA8650-05-D-5807, the NSF through Grant No. CHE-0809020, and the LANL LDRD Program. We would like to thank Kazuhiro Yanagi, Carter Kittrell, Wade Adams, Noe Alvarez, and Cary Pint for useful and stimulating discussions.

Supporting Information Available: Discussion of the remaining semiconducting (*n*,*m*) species present in the ME-SWNT sample through Raman and single-line excitation photoluminescence spectroscopies; observation of the (9,3) member of family $(2n + m) = 21$ *via* resonant Raman scattering using 514.5 nm excitation; and an explanation of how relative populations of specific (*n*,*m*) from Table 1 are calculated from Raman excitation profiles are provided. This material is available free of charge *via* the Internet at http://pubs.acs.org.

REFERENCES AND NOTES

1. Dekker, C. Carbon Nanotubes as Molecular Quantum Wires. *Phys. Today* **1999**, *52*, 22–28.
2. Baughman, R. H.; Zakhidov, A. A.; de Heer, W. A. Carbon Nanotubes—The Route toward Applications. *Science* **2002**, *297*, 787–792.
3. Ando, T.; Nakanishi, T. Impurity Scattering in Carbon Nanotubes—Absence of Back Scattering. *J. Phys. Soc. Jpn.* **1998**, *67*, 1704–1713.
4. White, C. T.; Todorov, T. N. Carbon Nanotubes as Long Ballistic Conductors. *Nature* **1998**, *393*, 240–242.
5. Tans, S. J.; Devoret, M. H.; Dai, H.; Thess, A.; Smalley, R. E.; Geerligs, L. J.; Dekker, C. Individual Single-Wall Carbon Nanotubes as Quantum Wires. *Nature* **1997**, *386*, 474–477.
6. Javey, A.; Guo, J.; Wang, Q.; Lundstrom, M.; Dai, H. Ballistic Carbon Nanotube Field-Effect Transistors. *Nature* **2003**, *424*, 654–657.
7. Arnold, M. S.; Stupp, S. I.; Hersam, M. C. Enrichment of Single-Walled Carbon Nanotubes by Diameter in Density Gradients. *Nano Lett.* **2005**, *5*, 713–718.
8. Arnold, M. S.; Green, A. A.; Hulvat, J. F.; Stupp, S. I.; Hersam, M. C. Sorting Carbon Nanotubes by Electronic Structure Using Density Differentiation. *Nat. Nanotechnol.* **2006**, *1*, 60–65.
9. Sato, Y.; Yanagi, K.; Miyata, Y.; Suenaga, K.; Kataura, H.; Iijima, S. Chiral-Angle Distribution for Separated Single-Walled Carbon Nanotubes. *Nano Lett.* **2008**, *8*, 3151–3154.
10. Yanagi, K.; Miyata, Y.; Kataura, H. Optical and Conductive Characteristics of Metallic Single-Wall Carbon Nanotubes with Three Basic Colors; Cyan, Magenta, and Yellow. *Appl. Phys. Exp.* **2008**, *1*, 034003.
11. Niyogi, S.; Densmore, C. G.; Doorn, S. K. Electrolyte Tuning of Surfactant Interfacial Behavior for Enhanced Density-Based Separations of Single-Walled Carbon Nanotubes. *J. Am. Chem. Soc.* **2009**, *131*, 1144–1153.
12. Miyata, Y.; Yanagi, K.; Maniwa, Y.; Kataura, H. Optical Evaluation of the Metal-to-Semiconductor Ratio of Single-Wall Carbon Nanotubes. *J. Phys. Chem. C* **2008**, *112*, 13187–13191.
13. Blackburn, J. L.; Barnes, T. M.; Beard, M. C.; Kim, Y. H.; Tenent, R. C.; McDonald, T. J.; To, B.; Coutts, T. J.; Heben, M. J. Transparent Conductive Single-Walled Carbon Nanotube Networks with Precisely Tunable Ratios of Semiconducting and Metallic Nanotubes. *ACS Nano* **2008**, *2*, 1266–1274.
14. Green, A. A.; Hersam, M. C. Colored Semitransparent Conductive Coatings Consisting of Monodisperse Metallic Single-Walled Carbon Nanotubes. *Nano Lett.* **2008**, *8*, 1417–1422.
15. Miyata, Y.; Yanagi, K.; Maniwa, Y.; Kataura, H. Highly Stabilized Conductivity of Metallic Single Wall Carbon Nanotube Thin Films. *J. Phys. Chem. C* **2008**, *112*, 3591–3596.
16. O'Connell, M. J.; Bachilo, S. M.; Huffman, C. B.; Moore, V. M.; Strano, M. S.; Haroz, E. H.; Rialon, K. L.; Boul, P. J.; Noon, W. H.; Kittrell, C.; Ma, J.; Hauge, R. H.; Weisman, R. B.; Smalley, R. E. Band-Gap Fluorescence from Individual Single-Walled Carbon Nanotubes. *Science* **2002**, *297*, 593–596.
17. Bachilo, S. M.; Strano, M. S.; Kittrell, C.; Hauge, R. H.; Smalley, R. E.; Weisman, R. B. Structure-Assigned Optical Spectra of Single-Walled Carbon Nanotubes. *Science* **2002**, *298*, 2361–2366.
18. Weisman, R. B.; Bachilo, S. M. Dependence of Optical Transition Energies on Structure for Single-Walled Carbon Nanotubes in Aqueous Suspension: An Empirical Kataura Plot. *Nano Lett.* **2003**, *3*, 1235–1238.
19. See the online Supporting Information for details.

20. Maultzsch, J.; Telg, H.; Reich, S.; Thomsen, C. Radial Breathing Mode of Single-Walled Carbon Nanotubes: Optical Transition Energies and Chiral-Index Assignment. *Phys. Rev. B* **2005**, *72*, 205438.
21. Fantini, C.; Jorio, A.; Souza, M.; Strano, M. S.; Dresselhaus, M. S.; Pimenta, M. A. Optical Transition Energies for Carbon Nanotubes from Resonant Raman Spectroscopy: Environment and Temperature Effects. *Phys. Rev. Lett.* **2004**, *93*, 147406.
22. Doorn, S. K.; Heller, D. A.; Barone, P. W.; Ursey, M. L.; Strano, M. S. Resonant Raman Excitation Profiles of Individually Dispersed Single-Walled Carbon Nanotubes in Solution. *Appl. Phys. A: Mater. Sci. Process.* **2004**, *78*, 1147–1155.
23. Jiang, J.; Saito, R.; Sato, K.; Park, J. S.; Samsonidze, Ge. G.; Jorio, A.; Dresselhaus, G.; Dresselhaus, M. S. Exciton−Photon, Exciton−Phonon Matrix Elements, and Resonant Raman Intensity of Single-Wall Carbon Nanotubes. *Phys. Rev. B* **2007**, *75*, 035405.
24. Ding, F.; Harutyunyan, A.; Yakobson, B. I. Dislocation Theory of Chirality-Controlled Nanotube Growth. *Proc. Natl. Acad. Sci. U.S.A.* **2009**, *106*, 2506–2509.
25. Strano, M. S.; Doorn, S. K.; Haroz, E. H.; Kittrell, C.; Hauge, R. H.; Smalley, R. E. Assignment of (*n,m*) Raman and Optical Features of Metallic Single-Walled Carbon Nanotubes. *Nano Lett.* **2003**, *3*, 1091–1096.
26. Machon, M.; Reich, S.; Telg, H.; Maultzsch, J.; Ordejón, P.; Thomsen, C. Strength of Radial Breathing Mode in Single-Walled Carbon Nanotubes. *Phys. Rev. B.* **2005**, *71*, 035416.
27. Goupalov, S. V.; Satishkumar, B. C.; Doorn, S. K. Excitation and Chirality Dependence of the Exciton−Phonon Coupling in Carbon Nanotubes. *Phys. Rev. B* **2006**, *73*, 115401.
28. Green, A. A.; Duch, M. C.; Hersam, M. C. Isolation of Single-Walled Carbon Nanotube Enantiomers by Density Differentiation. *Nano Res.* **2009**, *2*, 69–77.
29. Mukhopadhyay, S.; Maitra, U. Chemistry and Biology of Bile Acids. *Curr. Sci.* **2004**, *87*, 1666–1683.
30. Arnold, M. S.; Suntivich, J.; Stupp, S. I.; Hersam, M. C. Hydrodynamic Characterization of Surfactant Encapsulated Carbon Nanotubes Using an Analytical Ultracentrifuge. *ACS Nano* **2008**, *2*, 2291–2300.